International Journal of Modern Physics B
Vol. 31 (2017) 1750271 (11 pages)

DOI: 10.1142/S021797921750271X

Influence of nickel substitution on crystal structure and magnetic properties of strontium ferrite preparation via sol-gel auto-combustion route

Ebrahim Roohani[*,‡,§], Hadi Arabi[†] and Reza Sarhaddi[‡]

[*]*Department of Engineering, Bardaskan Branch, Islamic Azad University, Bardaskan, Iran*
[†]*Department of Physics, Faculty of Science, Ferdowsi University of Mashhad, Mashhad, Iran*
[‡]*Magnetism and Superconducting Research Laboratory, Department of Physics, University of Birjand, Birjand, Iran*
[§]*ebrahimroohani@yahoo.com*

Received 10 March 2017
Revised 16 June 2017
Accepted 28 June 2017
Published 8 August 2017

In this research, $SrFe_{12-x}Ni_xO_{19}$ ($x = 0 - 1$) hexagonal ferrites were prepared by sol-gel auto-combustion method. Effect of Ni substitution on structural, morphological and magnetic properties of nanoparticles was investigated by X-ray diffraction (XRD), Fourier transform infrared (FT-IR), Transmission electron microscopy (TEM) and vibrating sample magnetometer (VSM), respectively. The XRD results confirmed that all samples with $x \leq 0.5$ have single phase M-type strontium ferrite structure, whereas for the $SrFe_{12-x}Ni_xO_{19}$ samples with $x > 0.5$, the spinel $NiFe_2O_4$ phase has also appeared. The lattice parameters and crystallite sizes of the powders were concluded from the XRD data and Williamson–Hall method. Magnetic analyses showed that the coercivity of powders decreased from 5672 Oe to 639 Oe while the saturation magnetization increased from 74 emu/g to 81 emu/g with nickel substitution. The results of this study suggest that the strontium hexaferrites doped with Ni are suitable for applications in high density magnetic recording media as well as microwave devices because of their promising magnetic properties.

Keywords: M-type hexaferrite; strontium hexaferrite; Ni substitution; sol-gel auto-combustion; saturation magnetization; coercivity.

PACS numbers: 61.05.cp, 75.50.Bb, 75.50.Vv, 81.20.Fw, 81.70.Pg

[§]Corresponding author.

1. Introduction

There are a variety of hexagonal hard ferrites such as M, U, X, Y, Z, and W-type hexaferrites.[1–5] Among these materials, M-type hexagonal hard ferrites with general chemical formula $MFe_{12}O_{19}$ (M = Ba, Sr, Pb), have attracted great attention since their discovery in 1950s due to their extensive technological applications in magnetic recording media, permanent magnet, microwave and magneto-optical devices, and telecommunication. In addition, these materials are well known because of excellent chemical stability, corrosion resistivity, large saturation magnetization and coercivity, high Curie temperature, good thermal durability, and mechanical hardness.[6–11] The M-type strontium hexaferrite ($SrFe_{12}O_{19}$) can be prepared by several processes which are different in the production price and product properties. The most common and oldest method to synthesise strontium hexaferrite is using the solid-state reaction by blending of reactants (carbonates or oxides) and then calcining in a furnace at temperatures above 1200°C for periods of 2–8 h.[12] Solid-state technique has some inherent disadvantages such as chemical nonuniformity, large particle size and introduction of impurities during ball milling; furthermore, this method needs to use high-temperature furnaces with high energy consumption.[12,13]

To date, in order to obtain highly homogeneous M-type hexagonal ferrites, several methods such as co-precipitation, the traditional sol-gel, sol-gel autocombustion, glass crystallization, microemulsion, hydrothermal, organometallic and spray deposition have been developed and introduced to prepare the nanoparticles of strontium hexaferrite, though each one of these methods have their advantages and drawbacks.[12–15] Besides, in order to improve the magnetic and electrical properties of strontium hexaferrites and to make these materials suitable for different applications, researchers employed different strategies including the Fe^{3+}/Sr^{2+} mole ratio, heat treatment, pH of the starting solution, preparation method, and combinational substitution of different divalent, trivalent, and tetravalent metal cations in Sr and Fe sites.[16,17]

According to the literature, there is no report which studies in detail the influence of high doping content of nickel on structural, morphological and magnetic properties of strontium hexaferrite nanoparticles synthesized by sol-gel autocombustion method. Therefore, the main aim of the present study was to synthesize the nano size of strontium hexaferrite with the stoichiometry formula $SrFe_{12-x}Ni_xO_{19}$ by a suitable methodology to increase the saturation magnetization and decrease the coercivity simultaneously in order to make these materials suitable for application in high density recording media.

2. Experimental Details

2.1. *Materials and preparation method*

The chemicals used for the synthesis of $SrFe_{12-x}Ni_xO_{19}$ nanoparticle are as follows: Iron nitrate pentahydrate ($Fe(NO_3)_3 \cdot 9H_2O$), nickel nitrate hexahydrate

$Ni(NO_3)_2 \cdot 6H_2O$, and strontium nitrate anhydrous ($Sr(NO_3)_2$) as inorganic reactants, ammonium hydroxide as a neutralizing agent, citric acid as chelating agent, and deionized water as solvent. The starting materials were of high-purity compounds and used without further purification.

In this work, $SrFe_{12-x}Ni_xO_{19}$ ($x = 0$, 0.25, 0.5, 0.75, 1) hexagonal ferrites were prepared by sol-gel auto-combustion method as follows: first, the inorganic precursors including $Sr(NO_3)_2$, $Fe(NO_3)_3 \cdot 9H_2O$ and $Ni(NO_3)_2 \cdot 6H_2O$ in desired proportions corresponding to their stoichiometric formula ($SrFe_{12-x}Ni_xO_{19}$) were dissolved in deionized water by stirring on a hotplate at 50°C. Then temperature was increased slowly to 70°C and citric acid was added to the obtained sol with molar ratio of citric acid to total metal ions as 1:1. The resulting mixture was stirred for 30 min and afterward, the pH of solution was adjusted at 7 by adding ammonium hydroxide. Subsequently, the sol was heated on a hotplate with continuous stirring to evaporate the water until a highly viscous brown residue was formed. In the final step of the sol-gel auto-combustion process, the viscous residue was heated at 250°C for 1 h and then the obtained dark brown ashes were calcined at 1000°C for 5 h at a rate of 5°C/min.

2.2. *Powders characterization*

Fourier transform infrared (FT-IR) spectra of as-burnt and calcined powders were measured by a Shimadzu FTIR 4300 spectrometer in the range of 400–2000 cm^{-1}. The crystal structures of the powders were determined by the Bruker D8 Advance X-ray diffractometer using Cu-K_α radiation ($\lambda = 0.154056$ nm) with 2θ ranging from 20° to 80°. The morphology of the nanoparticles was investigated by transmission electron microscopy (TEM, LEO 912 AB) operating at 120 kV. The magnetic measurements of the calcined samples were carried out at room temperature with a vibrating sample magnetometer (VSM, Lake Shore 7400). The maximum applied field of 20 kOe has been used to evaluate the magnetic parameters of samples.

3. Results and Discussion

3.1. *FT-IR analysis*

Figure 1 shows FT-IR spectra of $SrFe_{12-x}Ni_xO_{19}$ ($x = 0 - 1$) calcined powders. In order to evaluate the effect of calcination temperature, the FT-IR spectrum of as-burnt $SrFe_{12}O_{19}$ powders which only dried at 250°C for 1 h, are also shown in Fig. 1. As can be seen, the most important peaks for as-burnt sample are at 1620 cm^{-1}, 1444 cm^{-1}, 874 cm^{-1} and 562 cm^{-1}, which correspond to the stretching and bending vibrations of C=O, H–C–H, C–C and C–N=O, respectively.[18] Furthermore, the FT-IR spectra of all calcined samples indicate three characteristics of vibration frequencies in the range 430–460 cm^{-1}, 550–560 cm^{-1} and 600–610 cm^{-1} corresponding to the formation of tetrahedral and octahedral clusters which confirms the presence of iron/nickel–oxygen stretching band in ferrites. In more detail, the

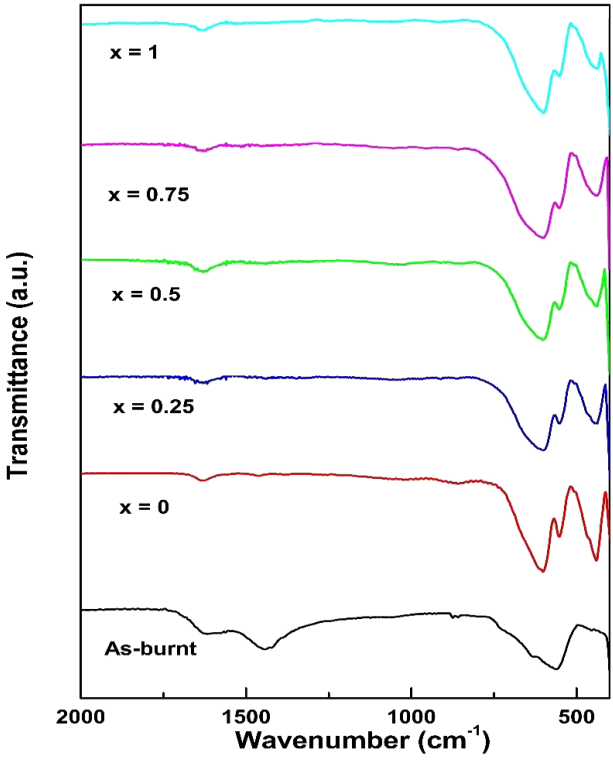

Fig. 1. (Color online) FT-IR spectra of $SrFe_{12-x}Ni_xO_{19}$ ($x = 0 - 1$) calcined powders together with as-burnt $SrFe_{12}O_{19}$ sample.

peaks in the range 430–460 cm^{-1} illustrate vibrations of octahedral bonds and other two peaks indicate tetrahedral. The vibrational modes of tetrahedral clusters are higher than that of octahedral clusters due to the shorter bond length of tetrahedral clusters.[19–21] It can also be observed that with the increase of nickel doping content (i.e., x), the value of FT-IR characteristic frequencies for $SrFe_{12-x}Ni_xO_{19}$ samples were shifted to a lower wavenumber due to Ni^{2+} ions with a heavier atomic weight than Fe^{3+} ions and the wavenumber being inversely proportional to the atomic weight.[22] Besides, the minor adsorption peak at 1625 cm^{-1} exhibits the stretch and bending bands of the surface hydrogen group (–OH) earned from wet atmosphere.[23] According to the mentioned results, it can be concluded that with the calcination of as-burnt powders at 1000°C, all of the organic compounds were completely eliminated, consequently bonds were formed between metals and oxygen that resulted in formation of crystal structure.

3.2. *XRD analysis*

The XRD patterns of $SrFe_{12-x}Ni_xO_{19}$ ($x = 0 - 1$) calcined powders are shown in Fig. 2. It can be seen that all samples with $x \leq 0.5$ have the hexagonal

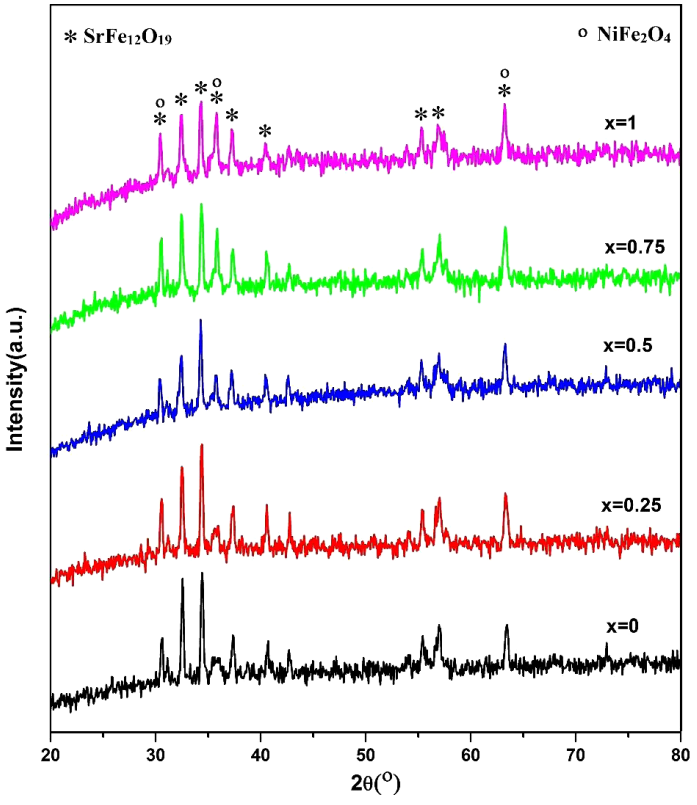

Fig. 2. (Color online) XRD patterns of $SrFe_{12-x}Ni_xO_{19}$ ($x = 0 - 1$) powders.

Magnetoplumbite structure (M-type) of strontium ferrite with space group $P6_3/mmc$ (No. 194), and the JCPDS card (#33-1340). There are no secondary peaks corresponding to extra phases like hematite which often appear at low temperatures when the reaction is not complete.[24] Therefore, it seems that Fe^{3+} ions are well substituted by Ni^{2+} ions in the crystallographic sites of the $SrFe_{12}O_{19}$ structure for $x \leq 0.5$. However, for the $SrFe_{12-x}Ni_xO_{19}$ samples with $x > 0.5$, the cubic nickel ferrite ($NiFe_2O_4$) phase with the JCPDS card No. 10-0325 has also appeared. As it is well known,[11,25,26] the structure of M-type hexagonal is stacked alternatively by spinel S [$Fe_6O_8^{2+}$] and hexagonal R [$MFe_6O_{11}^{2-}$] layers. The cubic spinel structure of $NiFe_2O_4$ is similar to the structure of S block of M-type hexagonal ferrites; therefore, it may be that the vacancy of $NiFe_2O_4$ has joined Fe^{3+} ions at the M-type hexagonal surface and the cubic structure of $NiFe_2O_4$ is formed. According to Iqbal *et al.*,[11] when synthesizing Ni-doped hexaferrites, it is hard to prevent the formation of nickel ferrite.

With increasing Ni doping value for $x \geq 0.5$, the intensity of the peaks of $NiFe_2O_4$ phase increases that demonstrates qualitatively an enhancement in the formation of cubic spinel structure as compared to pure hexagonal structure for

Table 1. Structural parameters of $SrFe_{12-x}Ni_xO_{19}$ ($x = 0 - 1$) calcined powders.

	$SrFe_{12}O_{19}$					$NiFe_2O_4$		
x	a (Å)	c (Å)	c/a	Crystallites size D (nm)	Weight fraction of phase (%)	a (Å)	Crystallites size D (nm)	Weight fraction of phase (%)
0	5.8637	23.0126	3.9246	49	100	—	—	0
0.25	5.852	22.9978	3.9223	50	100	—	—	0
0.5	5.851	23.0918	3.9389	52	100	—	—	0
0.75	5.865	23.1345	3.9467	54	97.1	8.3724	28	2.9
1	5.865	23.2521	3.9671	53	94.7	8.3718	26	5.3

$x < 0.5$.[27] In order to evaluate this result quantitatively, the XRD patterns of samples were submitted to a quantitative analysis by the Rietveld method using X'pert Highscore Plus software (Table 1).

The lattice constants for hexagonal and cubic phases ("a" and "c") were calculated from the XRD data using following formulae, respectively:

$$\frac{1}{d^2} = \frac{4}{3}\left(\frac{h^2 + hk + k^2}{\mathrm{a}^2}\right) + \frac{l^2}{\mathrm{c}^2}, \tag{1}$$

$$d = \frac{\mathrm{a}}{\sqrt{h^2 + k^2 + l^2}}, \tag{2}$$

where 'd' is the interplaner distance, 'hkl' are the Miller indices.[10,28,29] The crystallite size of samples was estimated by using the Williamson–Hall formula:

$$\beta \cos\theta = \frac{0.89\lambda}{D} + 2\varepsilon \sin\theta, \tag{3}$$

where 'λ' is the wavelength of the incident X-ray beam, 'θ' is the diffraction angle, 'β' presents the full-width half maximum of the Bragg peak, and ε is the strain, respectively. The obtained results are listed in Table 1.

As can be seen, the value of lattice constant "c" (except for $x = 0.25$) increases with an increase in Ni content, which can be due to the large ionic radius of Ni^{2+} ion (0.69 Å) than Fe^{3+} ion (0.64 Å).[30] For $x = 0.25$, the lattice constant "c" shows a decreasing trend, which is probably due to defects such as oxygen vacancies and lattice disorders. However, the value of lattice constant "a" nearly remains constant which is in agreement with the fact that all hexagonal types show constant lattice parameter "a" and variable parameter "c".[28,30] These results also indicate that the change of easy magnetized c-axis is larger than a-axis with Ni^{2+} ion substitution.[30] It has been reported that, the ratio of "c/a" may be used to determine the structure type of hexagonal hard ferrites, whereas the M-type hexagonal structure can be assumed if the ratio of "c/a" is observed to be less than 3.98.[31] From the results of Table 1, it is observed that the "c/a" values were calculated for all the $SrFe_{12-x}Ni_xO_{19}$ samples, ranged from 3.92 to 3.96, both well within the ratio range of M-type structures.

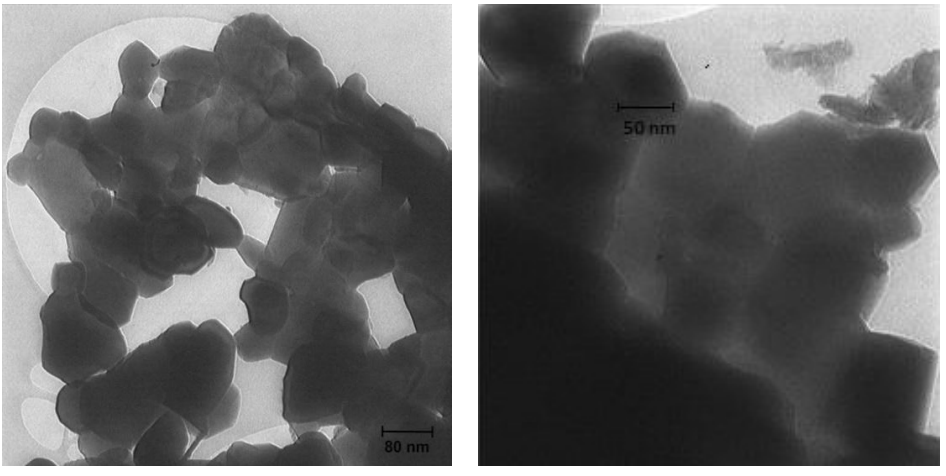

(a) (b)

Fig. 3. TEM images of $SrFe_{12-x}Ni_xO_{19}$ nanoparticles: (a) $x = 0$ and (b) $x = 0.5$.

The crystallites size of Ni-substituted strontium hexaferrite is found in the range of 49–55 nm, depending on the doping value. The variation of crystallite size with increasing nickel concentration demonstrates that the nickel doping value more than 0.75 inhibits the growth of crystals probably due to the grain boundary existences.[32] Besides, in the case of $SrFe_{12}O_{19}$, it was shown that the transition from single-domain to multi-domain structure is below 500 nm.[33] The D values of all the $SrFe_{12-x}Ni_xO_{19}$ samples are much smaller than the critical size (500 nm) of the single domain structure. Therefore, this result reveals that the particles with single-domain structure can be successfully prepared by using the sol-gel auto-combustion method.

3.3. *TEM analysis*

Figure 3 presents the TEM images of $SrFe_{12-x}Ni_xO_{19}$ ($x = 0$, 0.5) powders. As can be seen, the synthesized nanoparticles possess irregular shapes with both fine and large nanoparticles. The average grain size is found to be about 87–115 nm, whereas the Ni doping leads to a larger degree of crystal growth and therefore the bigger grains. Some of the particles are also agglomerated due to their magnetic nature. Furthermore, most of the grains are like platelets which are also observed for $BaFe_{12}O_{19}$ and $PbFe_{12}O_{19}$ hexaferrites.[34]

3.4. *Magnetic analysis*

Figure 4 shows the hysteresis loops for $SrFe_{12-x}Ni_xO_{19}$ ($x = 0 - 1$) samples measured at room temperature. The values of magnetic parameters such as saturation magnetization (M_s), remanent magnetization (M_r), squareness ratio (M_r/M_s), and

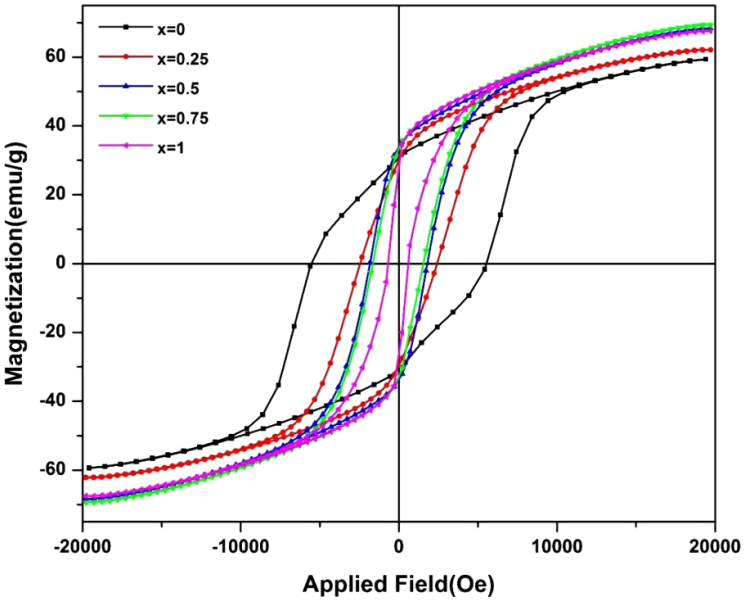

Fig. 4. (Color online) Hysteresis loops of $SrFe_{12-x}Ni_xO_{19}$ ($x = 0 - 1$).

Table 2. Magnetic parameters of $SrFe_{12-x}Ni_xO_{19}$ ($x = 0-1$) powders.

x	M_r (emu/g)	M_s (emu/g)	M_r/M_s	H_c (Oe)
0	33.50	74.26	0.451	5672
0.25	29.89	71.01	0.407	2431
0.5	33.84	80.36	0.421	1813
0.75	33.37	80.84	0.413	1601
1	27.58	78.01	0.353	639

coercivity (H_c) as a function of nickel doping value (x) are listed in Table 2. In spite of applying high magnetic field (20 kOe), the samples do not show the saturated magnetization, therefore, the saturation magnetization values were estimated from the extrapolation of M versus 1/H plots when 1/H go to zero.[35]

As shown in Fig. 5, the saturation magnetization continuously increases with Ni content up to $x \leq 0.75$ and then decreases slowly with further increase in the dopant content. This can be explained on the basis of the occupancy of nickel ions at different lattice sites of Sr-hexaferrite and also related to the super-exchange interaction strengths (Fe^{3+}–O–Fe^{3+}). In $SrFe_{12}O_{19}$ hexaferrite structure, out of 12 Fe^{3+} ions, eight have an upward spin at 12k, 2a, 2b and four a downward spin at $4f_1$ and $4f_2$ sites.[36,37] According to the configuration of Fe^{3+}, the four upward and four downward spins would cancel each other out, the remaining five unpaired electrons in the $3d$ orbital of the Fe^{3+} ions would have the magnetic moment of 5 μ_B, and the total moment for the four Fe^{3+} per formula units would therefore

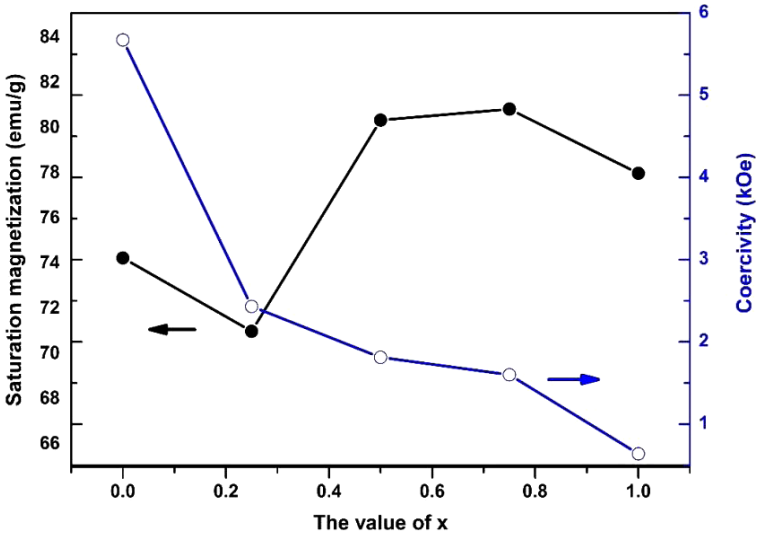

Fig. 5. (Color online) Variation of saturation magnetization and coercivity of $SrFe_{12-x}Ni_xO_{19}$ as a function of nickel doping (x).

be 20 μ_B. Accordingly, at substitution up to $x \leq 0.75$, Ni is expected to replace iron ions in the sites having spins in the downward direction ($4f_1$, $4f_2$). Since the magnetic moment of Ni^{2+} ions (2 μ_B) is smaller than that of Fe^{3+} ions (5 μ_B); therefore, the number of spin downs decrease which leads to enhancement of the saturation magnetization.[7,38] By increasing the dopant content of $x > 0.75$, Ni^{2+} ions are preferentially substituted in the 12k site; thus, the net spin of the Fe^{3+} ions in the upward direction decreases, and subsequently the saturation magnetization decreases. Furthermore, decrease in saturation magnetization for $x > 0.75$ may also be due to the appearance of the spinel structure of $NiFe_2O_4$ with soft magnetic properties which was identified before in XRD analysis section.

On the other hand, the coercivity (H_c) of the nanoparticles decreases continuously with the substitution of Ni^{2+} contents. It has been reported that the coercivity of M-type hexaferrites (SrM, BaM and PbM) depends on the particle size, porosity, the magnetocrystalline anisotropy.[35,36] It has also been reported that $4f_2$ and 2b sites contribute towards large anisotropy field and hence the coercivity.[38] In the present study, the coercivity of the nanoparticles continuously decreases from 5672 Oe to 639 Oe with the substitution of Ni^{2+} contents. The sharp decrease in coercivity value is directly related to the magnetocrystalline anisotropy constant that is principally related to the intrinsic effect associated with the substitution of Fe^{3+} ions by Ni^{2+} ions at both the $4f_2$ and 2b sites. Another reason for a decrease in coercivity of the samples, especially for substitution up to $x \leq 0.5$, can be attributed to an increase in grain size.[36]

Besides, the squareness ratio is essentially a measure of how square the hysteresis loop is and is given by the ratio of (M_r/M_s). In the present study, the

M_r/M_s values are found in the range of 0.353–0.451. In general, large M_r/M_s value is preferred in many applications such as magnetic recording media of high density and permanent magnets.[6] According to the literature study,[39] the longitudinal magnetic recording media (LMR) requires high enough coercivity (above 600 Oe). Furthermore, if the value of coercivity is above 1200 Oe, the material can be used for perpendicular recording media (PMR), which is a developing new technology in the magnetic recording media. In addition, the magnetic recording media require high magnetic remanence and high magnetic saturation to keep the recording information for a long time. In the present study, the coercivity values lie in the range from 5672 Oe to 639 Oe, the magnetic remanence, and magnetic saturation reached the highest values. So the $SrFe_{12-x}Ni_xO_{19}$ samples can be applicable in the perpendicular magnetic recording media and high density recording media.

4. Conclusion

In this study, strontium hexaferrite nanoparticles have been successfully prepared by sol-gel auto-combustion and the doping effect of nickel on the crystal structure and magnetic properties of $SrFe_{12-x}Ni_xO_{19}$ nanoparticles was investigated. The XRD diffraction patterns of nanoparticles approved the formation of $SrFe_{12}O_{19}$ single phase for $x \leq 0.5$, but for $x > 0.5$, small amounts of $NiFe_2O_4$ phase also appeared. The crystallite sizes were found in the range 49–54 nm. The FT-IR spectra of calcined samples showed three absorption peaks at bands 445, 560 and 610 cm^{-1} which confirms the presence of iron/nickel–oxygen stretching band in ferrites. The saturation magnetization (M_s) increases with the substitution of Fe^{3+} ions which attributed to the occupation of doped cation at Fe^{3+} ions site. The coercivity (H_c) of samples decreased with an increase in Ni^{2+} content due to the decrease of magnetocrystalline anisotropy and super-exchange interaction. The results show that these nanoparticles can be used at high density magnetic recording media because of their promising magnetic properties.

References

1. M. Y. Salunkhe *et al.*, *J. Magn. Magn. Mater.* **279**, 64 (2004).
2. M. A. Ahmed *et al.*, *J. Magn. Magn. Mater.* **320**, 1146 (2008).
3. M. C. Dimri *et al.*, *J. Ceram. Int.* **30**, 1623 (2004).
4. C. Wang *et al.*, *Mater. Sci. Eng. B* **99**, 270 (2003).
5. Y. Wu *et al.*, *J. Magn. Magn. Mater.* **324**, 616 (2012).
6. J. Z. F. Zi, Y. P. Sun, X. B. Zhu, Z. R. Yang, J. M. Dai and W. H. Song, *J. Magn. Magn. Mater.* **320**, 2746 (2008).
7. M. N. Ashiq *et al.*, *J. Magn. Magn. Mater.* **324**, 15 (2012).
8. M. J. Iqbal *et al.*, *J. Alloys Compd.* **478**, 736 (2009).
9. Y. Wang *et al.*, *J. Magn. Magn. Mater.* **321**, 3368 (2009).
10. M. N. Ashiq, M. J. Iqbal and I. H. Gul, *J. Magn. Magn. Mater.* **323**, 259 (2011).
11. M. J. Iqbal, M. N. Ashiq, P. Hernandez-Gomez, J. M. Munoz and C. T. Cabrera, *J. Alloys Compd.* **500**, 113 (2010).

12. K. S. Martirosyan, E. Galstyan, S. M. Hossain, Y.-J. Wang and D. Litvinov, *Mater. Sci. Eng. B* **176**, 8 (2011).
13. S. Alamolhoda, S. A. Seyyed Ebrahimi and A. Badiei, *J. Magn. Magn. Mater.* **303**, 69 (2006).
14. F. Song, X. Shen, J. Xiang and Y. Zhu, *J. Alloys Compd.* **507**, 297 (2010).
15. Y. Liu, G. B. Michael, B. Drew and Y. Liu, *J. Magn. Magn. Mater.* **323**, 945 (2011).
16. M. N. Ashiq, M. J. Iqbal and I. H. Gul, *J. Magn. Magn. Mater.* **323**, 259 (2011).
17. G. B. Teh, S. Nagalingam and D. A. Jefferson, *Mater. Chem. Phys.* **101**, 158 (2007).
18. M. G. Naseri, E. B. Saion, H. A. Ahangar, M. Hashim and A. Ha. Shaari, *Powder Technol.* **212**, 80 (2011).
19. M. Ghobeiti Hasab, S. A. Seyyed Ebrahimi and A. Badiei, *J. Non-Cryst. Solids* **353**, 814 (2007).
20. S. Singhal, T. Namgyal, J. Singh, K. Chandra and S. Bansal, *J. Ceram. Int.* **37**, 1833 (2011).
21. S. M. Masoudpanah and S. A. Seyyed Ebrahimi, *J. Magn. Magn. Mater.* **323**, 2643 (2011).
22. J. Xiang, X. Q. Shen, F. Z. Song and M. Q. Liu, *J. Solid State Chem.* **183**, 1239 (2010).
23. S. Kong *et al.*, *Particuology* **6**, 185 (2008).
24. E. Roohani, H. Arabi, R. Sarhaddi, S. Sudkhah and A. Shabani, *Int. J. Mod. Phys. B* **29**, 1550190 (2015).
25. S. Tyagi *et al.*, *J. Mater. Sci., Mater. Electron.* **22**, 1085 (2011).
26. S. Tyagi *et al.*, *J. Ceram. Int.* **37**, 2631 (2011).
27. A. I. Nandapure, S. B. Kondawar, P. S. Sawadh and B. I. Nandapure, *Physica B* **407**, 1104 (2012).
28. A. Sharbatiet *et al.*, *Solid State Commun.* **150**, 2218 (2010).
29. S. E. Mousavi Ghahfarokhi, S. Hosseini and M. Zargar Shoushtari, *Int. J. Min. Met. Mater.* **22**, 876 (2015).
30. S. Kanagesan, S. Jesurani, R. Velmurugan, S. Prabu and T. Kalaivani, *Mater. Res. Bull.* **47**, 188 (2012).
31. J. M. P. J. Verstegen and A. L. N. Stevels, *J. Lumin.* **9**, 406 (1974).
32. M. Liu, X. Shen, F. Song, J. Xiang and X. Meng, *J. Solid State Chem.* **184**, 871 (2011).
33. S. V. Ketov, Y. D. Yagodkin and V. P. Menushenkov, *J. Alloy. Compd.* **510**, 1065 (2011).
34. M. A. Ahmed, N. Helmy and S. I. El-Dek, *Mater. Res. Bull.* **48**, 3394 (2013).
35. Z. Durmus, *J. Nanomater.* **2014**, 302350 (2014), doi:10.1155/2014/302350.
36. M. J. Iqbal and S. Farooq, *Mater. Res. Bull.* **44**, 2050 (2009).
37. P. G. Bercoff, C. Herme and S. E. Jacobo, *J. Magn. Magn. Mater.* **321**, 2245 (2009).
38. M. J. Iqbal *et al.*, *J. Alloys Compd.* **505**, 560 (2010).
39. Y. Li, R. Liu, Z. B. Zhang and C. Xiong, *Mater. Chem. Phys.* **64**, 256 (2000).